The Structure of Turbulence in a Supersonic Shock-Wave/Boundary-Layer Interaction

Pascal L. Ardonceau*
Centre d'Etudes Aérodynamiques et Thermiques, Poitiers, France

This paper reports the experimental results from a detailed investigation of the turbulent flowfields in supersonic shock-wave/boundary-layer interactions at $M=2.25$. The interactions were produced by two-dimensional compression corners having angles of 8, 13, and 18 deg, the flows being respectively attached, incipiently separated, and separated. Turbulence data from a laser velocimeter and a constant-temperature, hot-wire anemometer are presented along with a mean flow survey from wall and pitot-static pressures. Qualitative aspects of the turbulence deduced from spectral analysis and high-speed schlieren pictures are also discussed. It is shown that a large amount of the turbulent energy is contained in large-scale structures that are still observed downstream of the interacting region, despite the severe pressure gradient. The lateral extent of these structures is of the order of one boundary-layer thickness and is roughly half of their longitudinal scale. A low-frequency unsteadiness is associated with the existence of a separation bubble, but does not affect the rest of the flow. The Reynolds shear stress is reduced in the vicinity of the separation bubble where the spatial derivatives of the normal stresses become significant.

Nomenclature

a'_w = hot-wire overheat ratio $= (R_w - R_w|_{T_t})/R_w|_{T_t}$
C = correlation coefficient
D = spectral density of energy
e,E = hot-wire output voltage
f = frequency
i = fringe spacing
M = Mach number
p = pressure
r = ratio between the sensitivity coefficient $S_{\rho u}/S_{T_t}$
R_w = hot-wire resistance
R_e = Reynolds number
$S_{\rho u}$ = hot-wire logarithmic sensitivity coefficient to mass flux
S_{T_t} = hot-wire logarithmic sensitivity coefficient to total temperature
T = temperature
u = longitudinal velocity component
v = normal velocity component
x = longitudinal coordinate, distance from hinge line of compression corner
y = distance normal to the model surface
z = transverse coordinate
α $= 1/(1+0.5(\gamma-1)M^2)$
β $= \alpha(\gamma-1)M^2$
γ = ratio of specific heats
δ = boundary-layer thickness
ρ = density
θ = angle with the x axis of the velocity component measured with the laser anemometer
$\langle\ \rangle$ = root mean square

Superscripts

$(\ )'$ = fluctuating value
$(\bar{\ })$ = time average

Subscripts

o = initial value ahead of interaction
t = total or stagnation condition
w = hot wire
∞ = freestream value ahead of interaction
δ = boundary-layer thickness

Received May 5, 1983; revision received Oct. 12, 1983.

*Research Scientist, Centre National de la Recherche Scientifique.

I. Introduction

THE computation of the flow across a shock-wave/boundary-layer interaction has been considered for many years, both as a computation of practical interest for applied aerodynamic configurations and as a test model for computational codes or for turbulence models. The efficiency of codes based on a direct solution of the Navier-Stokes equations has been shown[1,2]; however, at the present time there is not a closure of the time-average turbulent terms that can be considered satisfactory.[3] A large number of measurements based on the mean flow properties has been published and widely used,[4] but only few publications are devoted to the turbulent properties.[5-9] The aim of this paper is to contribute to the knowledge of the turbulence in such flows, particularly from a phenomenological point of view.

II. Description of Experiment

A. Wind Tunnel

The experiments were conducted in a square section, supersonic wind tunnel (150 × 150 mm) driven by a hypersonic ejector ($M=6$). The nozzle was designed to produce a Mach number of 2.25 in the test section. This moderate Mach number was selected to limit the compressibility effects on the turbulence, while being sufficiently high for the data reduction of the hot-wire output to be tractable (see Sec. II.E). The temperature was stabilized by a bed of small nickel balls located in the plenum chamber. The adiabatic condition for the walls was approximately achieved through a preheating of the nickel balls previous to the runs ($T_t \gtrsim 300$ K), insuring a recovery temperature very close to the room temperature. The stagnation pressure was 0.9 bar and the resulting Reynolds number was 1.1 10^7/m. The undisturbed boundary layer ($\delta_o \simeq 8$ mm) was found to be fully turbulent ($Re_\delta \simeq 10^5$) without any tripping.

B. Test Models

The various ways of generating a two-dimensional shock-wave/boundary-layer interaction may be broadly categorized

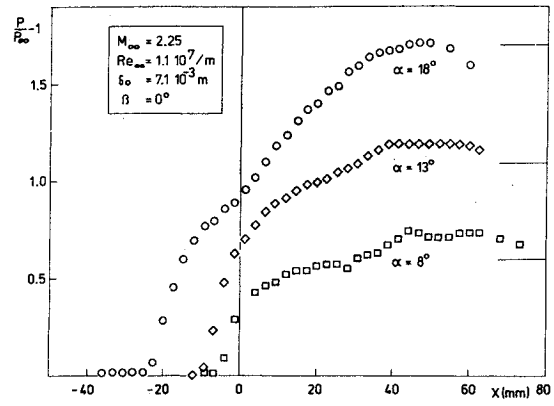

Fig. 1 Longitudinal surface pressure distributions for the three compression corners (8, 13, and 18 deg).

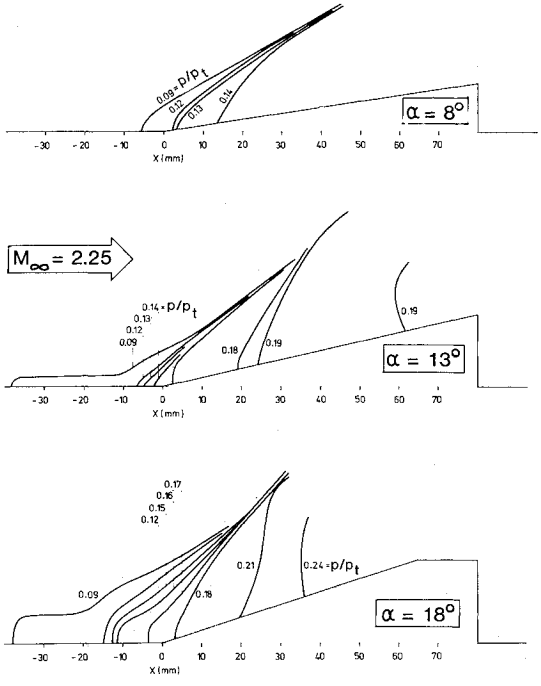

Fig. 2 Isobaric mapping of the static pressure for the three compression corners (8, 13, and 18 deg).

as 1) the incident shock method,[6,7] and 2) the compression corner method.[11] After some trials of models of the two categories with various geometries (full span, reduced span, models with fences, etc.), the full-span compression ramp was shown to generate a more stable and two-dimensional flow than the shock generator.[12] Moreover, there is no interaction between the shock wave and the expansion fan emanating from the trailing edge.[6] The ramp angle for incipient separation was estimated to be 13 deg,[13] and thus three ramps having angles of 8, 13, and 18 deg were selected to study the various flow regimes. The length of the compression corners was 80 mm, the maximum value that can be used without causing tunnel blockage.

C. Pressure Survey

The three models were instrumented along their centerline with a streamwise row of pressure taps (0.5 mm in diameter, 2.33 mm spacing). The surface pressure data measured from a mercury multimanometer are presented in Fig. 1. A typical "kink" on the 18 deg pressure distribution is observed and clearly indicates the presence of a flow separation. A

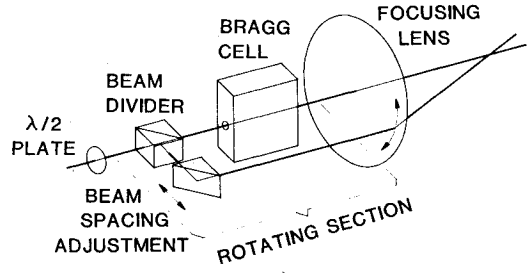

Fig. 3 Schematic of the LDA rotating beam divider.

moderate overshoot (as compared with the inviscid pressure levels) appears in the vicinity of $x = 40$ mm ($x = 0$ corresponds to the hinge line). The flow reaccelerates near $x = 60$ mm due to upstream influence from the trailing edge of the model. Additional spanwise pressure measurements and surface flow visualizations revealed good transverse uniformity of the flow. The lateral extent of the edge interactions was approximately 30 mm, leaving a 90 mm center part of the flow free from perturbations.[10]

Static and pitot pressure probing of the interacting boundary layer was carried out to validate the laser Doppler anemometer (LDA) data and to test the usual boundary-layer hypothesis of zero normal pressure gradient. The pressure probes (1.0 mm diam) had the same geometry as the hot-wire probe (DISA 55P11) to reproduce the same flow conditions even if interference occurred. The static probe was drilled with four 0.2 mm holes, at 12 diam from the nose. The front end of the pitot probe was flattened to limit displacement effects. The three probes were installed successively on the same probe support traversing the tunnel floor downstream of the models. The probes could be roughly aligned with the local flow direction by rotation of the probe support. The isobaric map of the static pressure (Fig. 2) clearly shows the focalization of the pressure waves outside of the boundary layer (δ varies at 8-12 mm). Two other features may be pointed out: 1) the inclination of the isobars is small near the wall but increases at the outer edge of the boundary layer, and 2) the influence of the compression extends far upstream in the inner part of the boundary layer. The velocity profiles deduced from the pressure measurements will be compared with the LDA data in the next section.

D. Laser Anemometry

Measurement Technique

A laser Doppler anemometer suitable for high-speed flows has been developed for the present study. The laser (Coherent Radiation CR6) was mounted on a movable bench with source and receiving optics on each side of the tunnel (dual forward scatter mode[14]). The beam divider (Fig. 3) included a Bragg cell (TSI model 580) to measure the reverse and normal flow components. The optical paths were nearly equal since the supplementary geometrical length of the lateral beam was compensated by the higher refractive index inside the Bragg cell. The fringe spacing was adjusted by moving the 90 deg prism to obtain a typical value of $i = 20$ μm. The beam divider could be rotated around the axis defined by the direct beam to select the proper sensing direction. A $\lambda/2$ plate located in front of the beam splitter was rotated at half the beam splitter angle to maintain a correct orientation of the polarization plane. The two beams were converged into the probe volume through a 600 mm focusing lens. The remainder of the setup included a high-aperture collecting lens and a photomultiplier (RCA XP 2001). The signal processing was achieved by a digital counter (TSI model 1990) connected to a Norsk Data 100 computer. Seeding of the flow in the plenum chamber by a DOP generator[15] was found convenient to increase the rate of data acquisition to approximately 3000 s^{-1}. The statistical

results were based on 1000 instantaneous frequency readings and the widely used 3σ test[7] was applied to eliminate erroneous data.

The procedure adopted to measure the two velocity components and the Reynolds stresses made use of the directional sensitivity of the LDA. If θ is the angle of the perpendicular to the fringe plane with the x axis of a given x, y frame of reference, a simple relationship can be obtained between the rms frequency measured in the θ position and the rms velocity components,

$$i\cdot\langle f'(\theta)\rangle^2 = \langle u'\rangle^2\cos^2\theta + \langle v'\rangle^2\sin^2\theta + 2\overline{u'v'}\sin\theta\cos\theta \quad (1)$$

The three unknowns may be deduced from successive measurements of $\langle f'(\theta)\rangle$ at three different angles, for instance 0, 45, and 135 deg.[16] However, to reduce the statistical uncertainty arising from data differencing, $\langle f'(\theta)\rangle$ was measured at six different angles α: 0, 50, 70, 90, 110, and 130 deg and a least-squares regression method was applied to find the values of the three unknowns from the redundant system of six equations. A typical result is presented in Fig. 4. The method was found to perform well. The main advantage is that a single-channel processor is required instead of a two-channel setup when the two velocity components are to be measured simultaneously. The increase of the tunnel running time due to taking six successive measurements, by comparison with a simultaneous two-channel procedure, was partly compensated for, because the method required less operation (filter and threshold tuning) and also the number of data rejections was comparatively much smaller.

Results

Results have been obtained for three ramp angles. Since no particular effects were associated with the occurrence of separation, the data selected for this paper concern the 18 deg ramp angle.

Nine profiles were investigated with the laser anemometer. The locations were: -36, -20, -12, -4, $+4$, $+12$, $+20$, $+36$, and $+52$ mm from the hinge line of the compression corner. A comparison between the velocity deduced from the pitot tube and the laser is presented in Fig. 5 for some typical profiles. The modulus of the mean velocity from LDA data is plotted, rather than the longitudinal component in order to match more accurately the pitot tube results. The overall comparison is farily good; however, some discrepancies may be noticed near the wall on the $x=+4$ mm profile. The laser gives higher velocities than the pitot tube, despite the processing applied to the LDA data to correct for the sampling bias due to the averaging process.[17] The misalignment of the pressure probes, especially the static probe, does not seem sufficient to explain the discrepancies and the turbulence effects on the pressure measurements should lead to overestimation of the mean velocity.[10,25] It is strongly felt that some kind of bias with the LDA arises from a lower seeding level near the wall (and consequently along the separation streamline).

The longitudinal and normal rms velocities are plotted in Figs. 6 and 7. The influence of the compression is noticeable on the profiles at $x=-12$ mm. The longitudinal velocity component reacts more strongly than the normal component, particularly in the inner part of the boundary layer. With increasing longitudinal distance, the fluctuating region spreads toward the outer part of the boundary layer and a maximum appears at 3-4 mm from the wall. The ratio between $\langle u'\rangle$ and $\langle v'\rangle$ become higher than the quilibrium value in the profiles at $x=-12$ and -4 mm, but returns to the typical value of 2 downstream. On the last measured profiles, the fluctuation level is still two to three times the value in the undisturbed boundary layer. The dissipation process of the large eddies would require a much longer distance.

The Reynolds shear stress profiles are presented in Fig. 8. The velocity components as well as $\overline{u'v'}$ were computed in a frame of reference with the longitudinal axis parallel to the wall. The convention may look arbitrary but has been preferred to an orientation of the frame of reference relative to the mean flow direction, since the latter is not accurately defined near the separation bubble.

The overall increase of $\overline{u'v'}$ is quite noticeable. While the increase of the rms velocities $\langle u'\rangle$ and $\langle v'\rangle$ contributes greatly to this result, the correlation coefficient $C_{uv}=\overline{u'v'}/\langle u'\rangle\cdot\langle v'\rangle$ is also considerably modified. An average value of $C_{uv}=-0.4$ (deduced from data of Figs. 6-8) is observed on the first profile. A very large negative value, close to -1.0, is measured in the vicinity of the separation shock and follows from the unsteady motion of the shock wave (see Sec. II.F). Near the wall, C_{uv} tends to decrease down to the corner hinge line, but recovers an average value of $\simeq -0.6$ in the main part of the boundary layer farther downstream. Returning to the shear stresses $\overline{u'v'}$, a decrease may be noticed on the last measured profiles, while there is no corresponding decrease of the turbulence intensities. It may be argued that the organized turbulent motion, which is

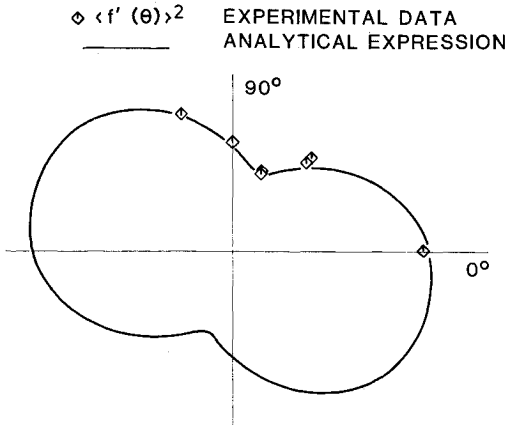

Fig. 4 Polar representation of the squared rms frequency as measured with the rotating LDA sensor (comparison with the analytical expression is deduced from measurements).

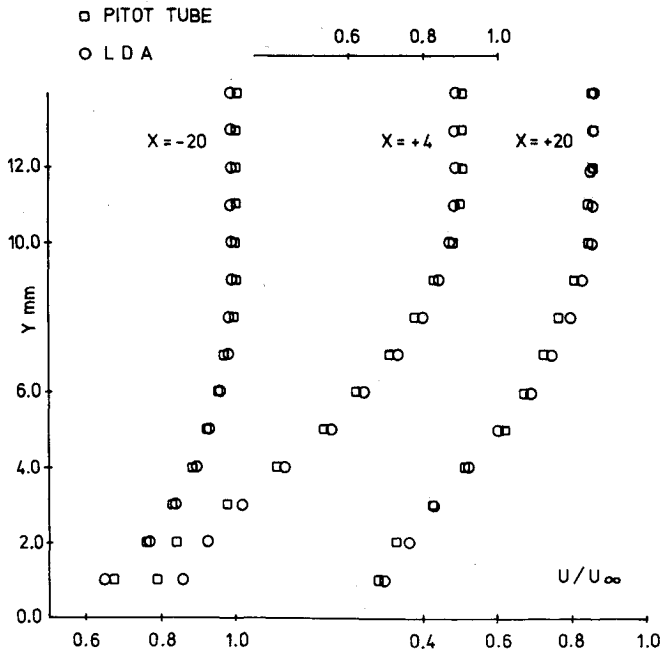

Fig. 5 Comparison between the mean velocity (modulus) deduced from pitot tube and LDA (18 deg ramp angle).

responsible for the rapid reacceleration of the inner part of the boundary layer, degenerates in a short distance as compared to the length necessary to dissipate the large structures. The appearance of the flow on some schlieren pictures seems to support this hypothesis (see Sec. II.F). The existence of a maximum of $\overline{u'v'}$ relatively distant from the wall has been observed elsewhere in supersonic flows[6,7] but also in subsonic separating boundary layers[18] where the turbulence exhibits a similar behavior.

E. Hot-Wire Anemometer

Measurement Procedure

The laser Doppler anemometer was able to furnish interesting quantitative results, but only of a statistical nature due to the sampling procedure. Some fundamental and more qualitative aspects of the turbulence structure were investigated by use of a constant-temperature, single hot-wire anemometer. The instantaneous wire response $e'(t)$ is supposed to depend linearly upon the turbulent fluctuations of density ρ', longitudinal velocity u', and total temperature T_t' (small perturbations: $\langle e' \rangle / \bar{E} \ll 1$). Following the Morkovin-Kovasznay analysis[19,20] the dependent contributions of the two variables ρ' and u' may be gathered into a single variable, the mass flux $\rho u'$, provided that the Mach number is high enough[19] ($M<1.4$). Logarithmic sensitivity coefficients are introduced as

$$S_{\rho u} = \frac{\partial \log \bar{E}}{\partial \log \overline{\rho u}}\bigg|_{R_w, \bar{T}_t} \qquad S_{T_t} = -\frac{\partial \log \bar{E}}{\partial \log \bar{T}_t}\bigg|_{R_w, \overline{\rho u}}$$

and the instantaneous linear relationship between e', $\rho u'$, and T_t' may be written

$$\frac{e'(t)}{\bar{E}} = S_{\rho u}\frac{\rho u'}{\overline{\rho u}} - S_{T_t}\frac{T_t'}{\bar{T}_t} \tag{2}$$

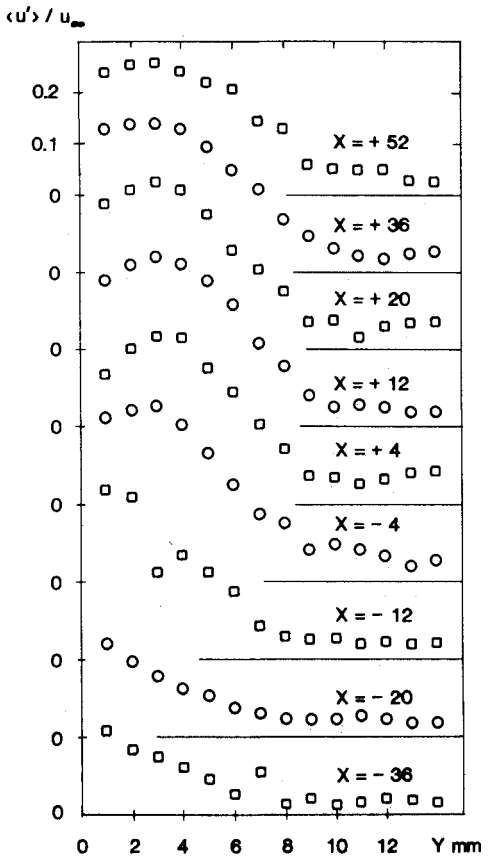

Fig. 6 Longitudinal rms velocity (18 deg ramp angle).

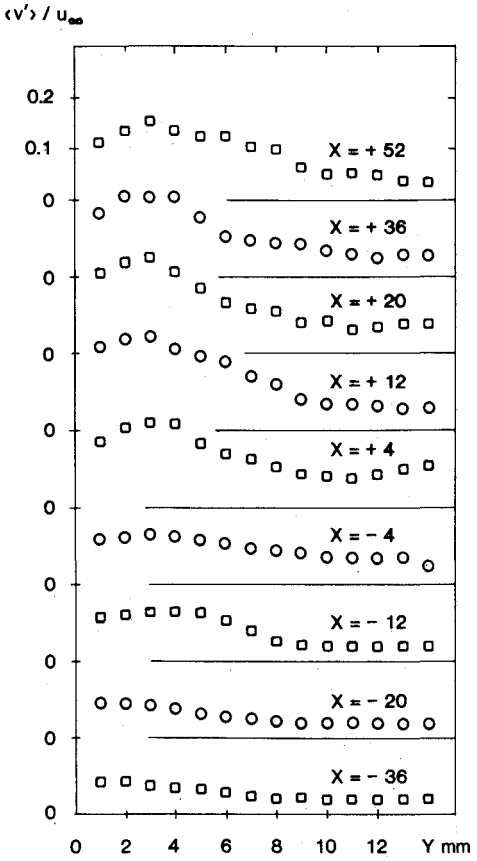

Fig. 7 Normal rms velocity (18 deg ramp angle).

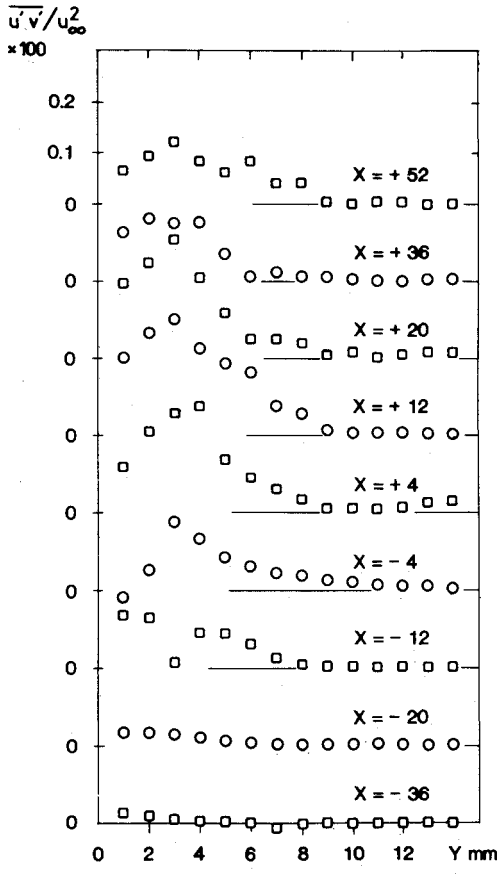

Fig. 8 Reynolds shear stresses (18 deg ramp angle).

which becomes after a time integration of the squared relation,

$$\frac{\langle e' \rangle^2}{\bar{E}^2} = S_{\rho u}^2 \frac{\langle \rho u' \rangle^2}{\overline{\rho u}^2} + S_{T_t}^2 \frac{\langle T_t' \rangle^2}{\bar{T}_t^2} - 2CS_{\rho u} S_{T_t} \frac{\langle \rho u' \rangle \langle T_t' \rangle}{\overline{\rho u} \cdot \bar{T}_t} \quad (3)$$

where $C = (\overline{\rho u' \cdot T_t'}) / (\langle \rho u' \rangle \langle T_t' \rangle)$ is the correlation coefficient between $\rho u'$ and T_t'.

This widely used method in supersonic flow relies on the fact that $S_{\rho u}$ and S_{T_t} depend upon the wire heating. From successive experiments (≥ 3) with different overheat ratios, $\langle \rho u' \rangle \langle T_t' \rangle$ and C may be deduced. The probes were calibrated in a special supersonic calibration tunnel[21] (section 20×20 mm, Mach number 2.5) that was designed in order to generate a quasilinear variation of M with the distance from the nozzle. The variations of ρu were achieved by displacing the probe along the nozzle axis, while the variations of the total temperature were obtained by electrical heating of the flow. The stagnation pressure was adjusted to reach a typical Reynolds number based on the wire diameter of 55.

The anemometer, a DISA M55, was equipped with a symmetrical 55M12 bridge that had been shown to be more stable at high frequency than the standard bridge. The probes were DISA 55P11 with a reduced gap of 1 mm between the prongs and a 5 μm wire, slack welded to avoid parasitic strain gage effects.[21]

The sensitivity coefficients are plotted in Fig. 9. A slight linear variation of $S_{\rho u}$ with the mass flux ρu may be observed, while there is almost no influence of the overheat of the wire (the spread of the results for the range of overheat ratios used during the experiments and for six different probes lies within the dashed lines). The value of $S_{\rho u}$ is in very close agreement with the incompressible value of 0.25 that follows from the law of King. S_{T_t} is plotted vs the overheat ratio rather than the mass flux, since there is only a slight effect of ρu. The presentation of S_{T_t} vs a_w' implicitly assumes that the heat transfer between the wire and the flow depends upon the difference $(T_w - T_t)$ rather than upon T_w and T_t independently. Only small variations of T_t were expected and the hypothesis was therefore justified. It is noticeable that, even for the higher overheat ratio, S_{T_t} remains at least twice as great as $S_{\rho u}$. Thus, the contribution of small fluctuations of T_t to the wire response could not be neglected.

Since the frequency limit of the anemometer appeared to be strongly dependent upon the overheat ratio, a careful test was undertaken to define the lower limit of the overheat ratio compatible with the turbulent fluctuation spectrum. An optical unsteady heating of the probe by means of a modulated laser beam was preferred to the usual square wave test. The details of the method are presented in Ref. 22. Results for three heatings of the wire are presented in Fig. 10. The optimal settings of gain and frequency cutoff were used in each case. While a very good frequency response is observed for $a_w' = 0.75$ ($f_{3dB} > 300$ kHz), the upper frequency limit does not exceed 100 kHz when $a_w' = 0.26$. A method of data regression has been developed to measure the more important of the two variables, namely $\langle \rho u' \rangle$, without neglecting the contribution of $\langle T_t' \rangle$. This was achieved through a differential procedure using high and medium overheat ratios ($0.8 < a_w' < 0.4$).

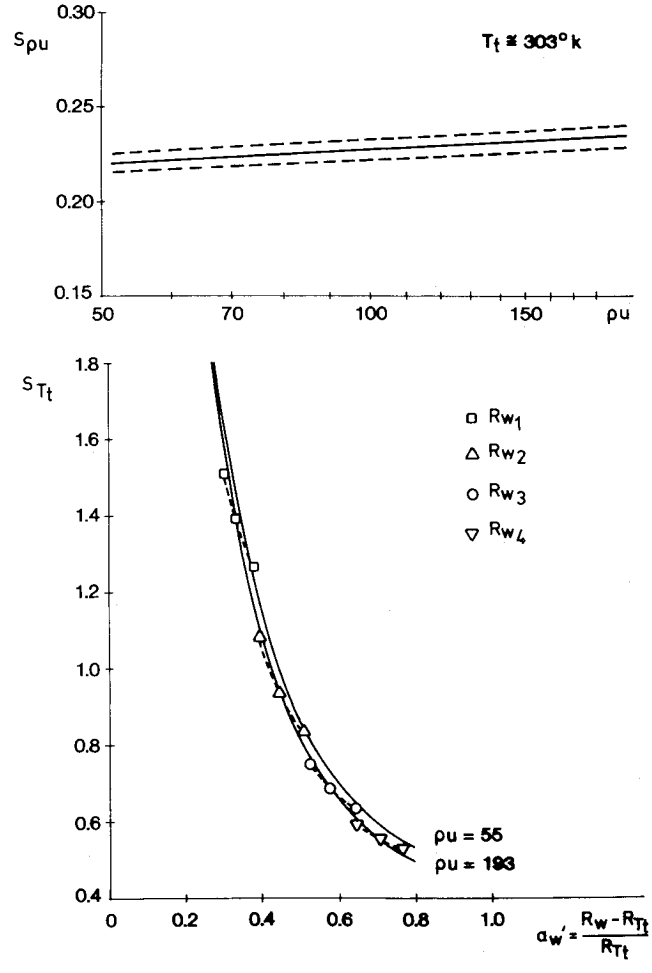

Fig. 9 Hot-wire sensitivity coefficients deduced from calibration tests.

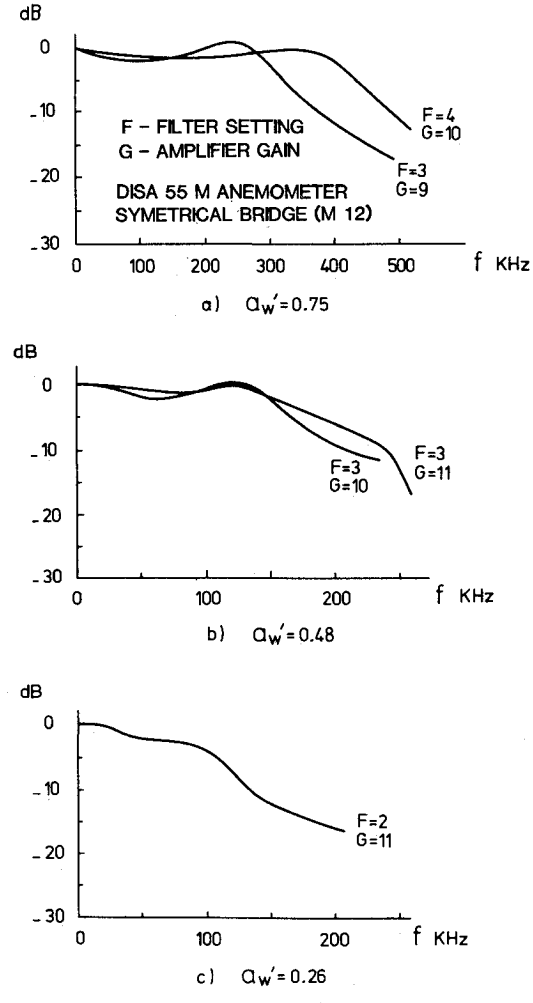

Fig. 10 Dependence upon the overheat of the hot-wire anemometer frequency response.

The relation between $\langle e' \rangle$, $\langle \rho u' \rangle$, and $\langle T_t' \rangle$ may be written as a function of the ratio $r = S_{\rho u}/S_{T_t}$,

$$\frac{1}{S_{T_t}}\frac{\langle e' \rangle^2}{\bar{E}^2} = r^2 \frac{\langle \rho u' \rangle^2}{\overline{\rho u}^2} + \frac{\langle T_t' \rangle^2}{\bar{T}_t^2} = -2rC \frac{\langle \rho u' \rangle \langle T_t' \rangle}{\overline{\rho u} \bar{T}_t} \quad (4)$$

and

$$\frac{1}{S_{T_t}}\frac{\langle e' \rangle}{\bar{E}} = r\frac{\langle \rho u' \rangle}{\overline{\rho u}}\left(1 - \frac{2C}{r}\frac{\langle T_t' \rangle}{\bar{T}_t}\Big/\frac{\langle \rho u' \rangle}{\overline{\rho u}} + \frac{1}{r}\frac{\langle T_t' \rangle^2}{\bar{T}_t^2}\Big/\frac{\langle \rho u' \rangle^2}{\overline{\rho u}^2}\right)^{1/2} \quad (5)$$

It has been shown[12] for the experimental data that the ratio between $\langle T_t' \rangle/\bar{T}_t$ and $\langle \rho u' \rangle/\overline{\rho u}$ is small since $\langle T_t' \rangle/\bar{T}_t$ did not exceed 0.015 in the interacting boundary layer at $M = 2.25$. The quantities appearing in the right side of Eq. (5), i.e., r, C, and $\langle \rho u' \rangle/\overline{\rho u}$ have been shown from experience to be of 0(1). Then, neglecting the $0(\epsilon^2)$ term in Eq. (5) and replacing $(1-2\epsilon)^{1/2}$ by $1-\epsilon$ gives

$$\frac{1}{S_{T_t}}\frac{\langle e' \rangle}{\bar{E}} = r\frac{\langle \rho u' \rangle}{\overline{\rho u}} - C\frac{\langle T_t' \rangle}{\bar{T}_t} \quad (6)$$

This expression, valid provided that r is not too small, is the asymptotic value of Eq. (5) for large r ($r > 0.25$). Since C and $\langle T_t' \rangle/\bar{T}_t$ are not meaningful quantities, they were not considered independently, and the mass flux fluctuations have been deduced from only two measurements with $r \simeq 0.25$ and $\simeq 0.4$ corresponding to an overheat ratio of 0.4 and 0.8. A cruder estimation is sometimes made that neglects the product $C \cdot \langle T_t' \rangle/\bar{T}_t$. Then,

$$\frac{\langle e' \rangle}{\bar{E}} = S_{\rho u}\frac{\langle \rho u' \rangle}{\overline{\rho u}} \quad (7)$$

The rms mass flux has been estimated from Eqs. (7), (6), and (5) using, respectively one, two, and seven different overheat ratios in the case of an undisturbed boundary layer (Fig. 11). There is a close agreement between the two methods that did not neglect the effect of $\langle T_t' \rangle$, while the simplest is shown to highly underpredict $\langle \rho u' \rangle$. Therefore, the linear method of Eq. (6) has been chosen as being of similar accuracy to, but less time-consuming than, the full identification procedure, while Eq. (7) is rejected as being inaccurate.

Mach Number Influence

The analysis of the hot-wire response that has led (ρu) to be considered as a single variable is known to be valid for supersonic Mach numbers.[23] In order to check the limits of the analysis, a calibration of the hot wire has been made for several transonic Mach numbers. The probe was then fixed near the nozzle of the tunnel and the mass flux varied by changing the stagnation pressure. The mass flux sensitivity coefficient $S_{\rho u}$ is plotted in Fig. 12 against the Mach number. As may be seen, there is a strong dependence near $M \simeq 1$, which may be attributed to the displacement of a detached shock wave emanating from the prongs and interacting with the hot wire. Since no particular dependence of $S_{\rho u}$ with M was introduced in the data regression procedure, the data corresponding to Mach numbers in the limit $0.8 < M < 1.4$ must be considered with much care.[24]

Results

The rms mass flux in the interacting boundary layer is plotted Fig. 13. The points corresponding to a mean Mach number less than 1.5 are plotted distinctively. A rapid increase of $\langle \rho u' \rangle$ with distance may be observed at the 18 deg ramp angle: the fluctuation level is mutiplied by nearly five in a distance of the order of 4 δ_o. It may be noticed that, although the final pressure level is reached in a short distance (Fig. 1),

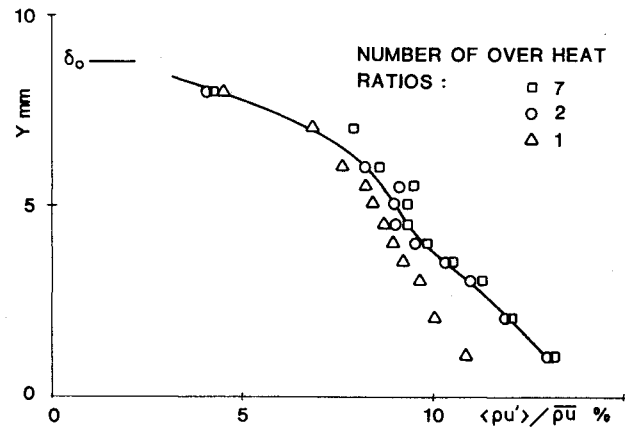

Fig. 11 Rms mass flux in the undisturbed boundary layer deduced from different hot-wire data reduction methods (△ $a_w' = 0.75$; ○ $a_w' = 0.53, 0.75$; □ $a_w' = 0.25, 0.27, 0.31, 0.37, 0.53, 0.63, 0.75$).

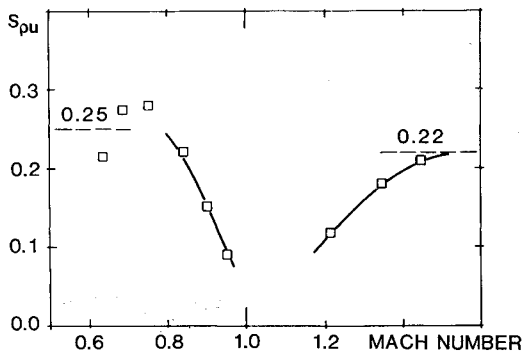

Fig. 12 Relation between the mass flux sensitivity coefficient and the Mach number in the transonic range.

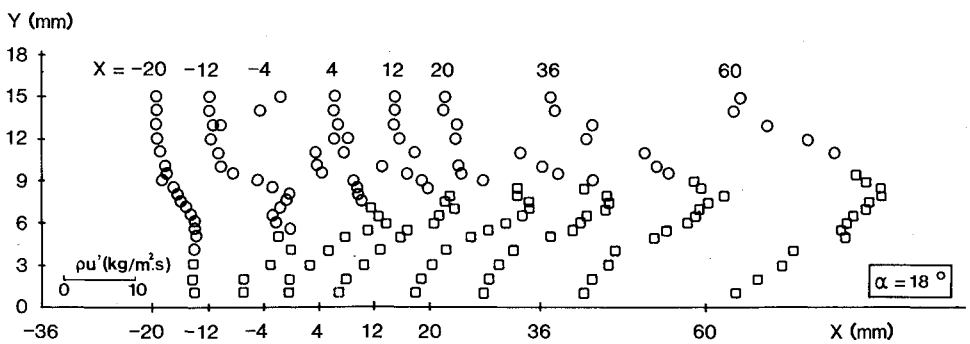

Fig. 13 Rms mass flux in the interacting flowfield (○ local Mach number > 1.5, □ local Mach number < 1.5).

the fluctuations remain quite strong in the last measured profiles. The reorganization of the turbulence would take a longer distance than the maximum length of compression corner that can be used without causing tunnel blockage.

The velocity fluctuations may be deduced from hot-wire data if the assumption $\langle p' \rangle / \bar{p} \ll 1$ is made[19]

$$\frac{\langle u' \rangle}{\bar{u}} = \frac{1}{\alpha+\beta}\left(\alpha^2 \frac{\langle \rho u' \rangle^2}{\overline{\rho u}^2} + \frac{\langle T_t' \rangle^2}{\bar{T}_t^2} + 2\alpha \frac{\langle \rho u' \rangle}{\overline{\rho u}} \frac{\langle T_t' \rangle}{\bar{T}_t} C\right)^{1/2} \quad (8)$$

where

$$\alpha = \frac{1}{1+(\gamma-1)M^2/2} \quad \text{and} \quad \beta = \alpha(\gamma-1)M^2$$

If $\langle T_t' \rangle / \bar{T}_t$ is further neglected the expression simplifies into

$$\frac{\langle u' \rangle}{\bar{u}} = \frac{1}{1+(\gamma-1)M^2} \frac{\langle \rho u' \rangle}{\overline{\rho u}} \quad (9)$$

A comparison between LDA and hot-wire data for a sample of rms longitudinal velocity profiles is presented in Fig. 14. As could be deduced from the strong dependence of $S_{\rho u}$ on Mach number in the transonic range, large discrepancies occur for $M<1.5$. The underestimation of $\langle u' \rangle$ as measured with the hot wire is in agreement with the overestimation of $S_{\rho u}$, which may decrease to less than half its estimated value in supersonic flow. In the regions where $M>1.5$, there is a fairly good agreement between the two methods. Hot-wire anemometer results are therefore quantitatively unreliable in the transonic range unless a special calibration is made to allow for the Mach number dependence. The presence of non-negligible fluctuating pressure levels[26] casts some doubt upon the hypothesis that $\langle p' \rangle / \bar{p} \ll 1$.

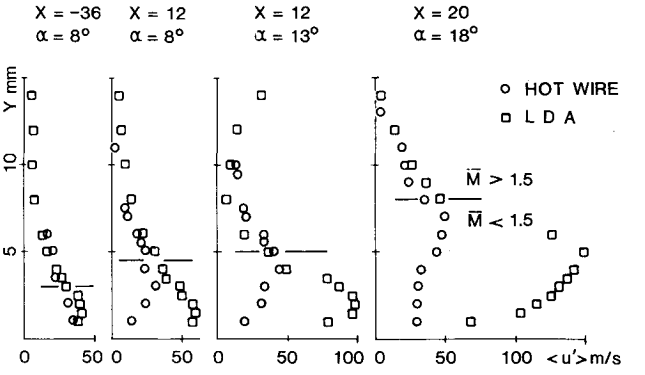

Fig. 14 Comparison between the rms longitudinal velocity deduced from LDA and hot-wire data ($\langle p' \rangle = 0$).

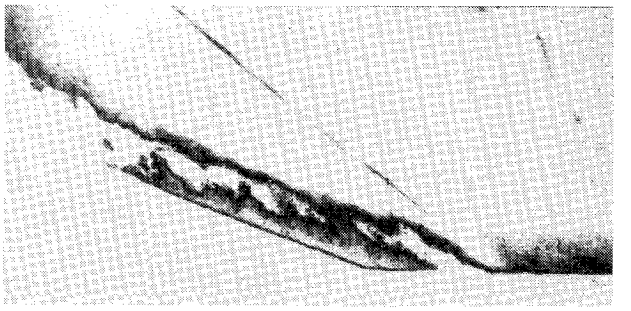

Fig. 15 High-speed schlieren picture of the interaction (exposure time ~2 μs).

F. The Structure of Turbulence

Optical Flow Visualization

From the observation and image analysis of high-speed schlieren photographs, it seemed obvious that large-scale structures were present in the flow ahead and even downstream of the strong compression from the shock wave. Figure 15 reproduces the false color imaging from a black-and-white schlieren picture of the flow. The most striking feature is the appearance of a quasiperiodic vortex sheet emanating from the foot of the shock wave, which spreads slightly behind the separation bubble. Although no definite conclusion can be drawn, it is supposed that the lateral extension of these structures is large, since the schlieren technique integrates over the width of the tunnel (which is roughly 15 times the boundary-layer thickness).

Longitudinal Structure of Turbulence

The longitudinal properties of the turbulent structures have been investigated by means of spectral analysis of the instantaneous hot-wire signal. Since the total temperature fluctuations were small and the hot wire was set to the maximum overheat ($\simeq 0.8$), the hot-wire signal was assumed to represent $\rho u'(t)$. The spectral density of the fluctuations $D(f)$ has been multiplied by the frequency and the result is plotted on a semilogarithmic scale. Then

$$\int_{f_1}^{f_2} f \cdot D(f) \cdot \mathrm{d}(\log f) = \int_{f_1}^{f_2} D(f) \cdot \mathrm{d}f \quad (10)$$

The amount of energy contained in a frequency band f_1, f_2 is then directly related to the area of the curve delimited by these frequencies. A sample of representative spectra is given in Fig. 16. In the undisturbed boundary layer, the main part of the energy is included at 10-50 kHz with a maximum located at 20 kHz. A corresponding longitudinal scale of $\simeq 2\delta_o$ can be deduced by means of the Taylor hypothesis of convection of a frozen pattern of turbulence.

A low-frequency component appears very close to the separation bubble. This component cannot be related to a turbulent property since the associated longitudinal macroscale should be ~50 times the boundary-layer thickness. This phenomenon is more probably a consequence of an unsteady property of the separation bubble, giving rise to a low-frequency motion of the streamlines that induces large variations of the hot-wire output, since $\partial \overline{\rho u}/\partial y$ is large in that region. To support the hypothesis of a nonturbulent contribution, it may be observed that the low-frequency component is not convected downstream of the separation bubble.

Another interesting feature is the close qualitative similarity of the spectra upstream and downstream of the interaction. The energy of the turbulence seems to be reinforced in the same manner throughout the spectrum. Consequently, it may be emphasized that the large-scale structures of the undisturbed boundary layer do not loose their coherence during the interaction with the mean velocity field. More likely, there is an energy transfer from the mean flow to the turbulent structures, which are then able to accelerate the inner part of the retarded boundary layer through the turbulent mixing.

Lateral Properties

The lateral aspect of the turbulent structures has been investigated by means of the lateral correlation function of the longitudinal mass flux fluctuations $C_{\rho u', \rho u'}(\Delta z)|_{x,y,z}$. Two hot-wire probes were operated at the same time at a high overheat ratio, and the outputs were analogically correlated through a DISA 55B25 turbulence processor. One of the probes was held fixed and the other moved laterally from $z=2$ mm to approximately 20 mm. A first test was done at a variable height in the undisturbed boundary layer (Fig. 17). The correlation functions present a well-defined negative value for spacings ranging 4-5 mm at $y=2$ mm and 4-6 mm at

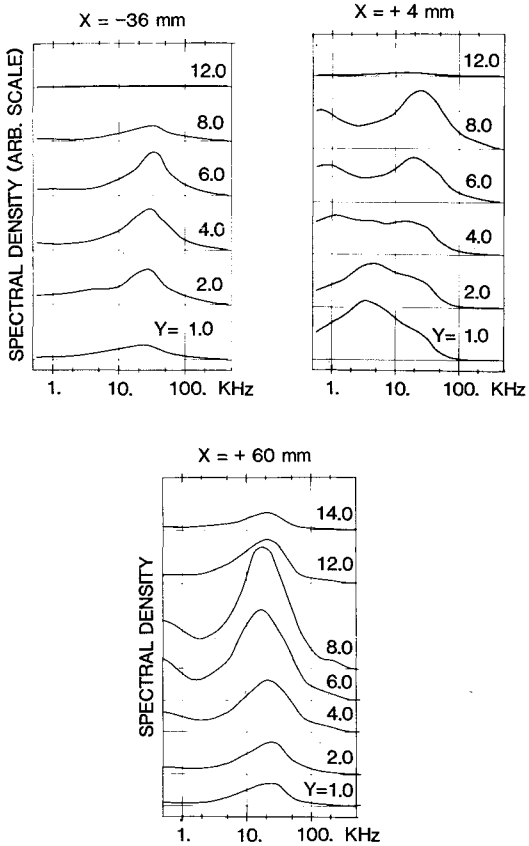

Fig. 16 Spectral analysis of the hot-wire output voltage at various locations [$f.E(f)$ is plotted against $\log_{10} f$].

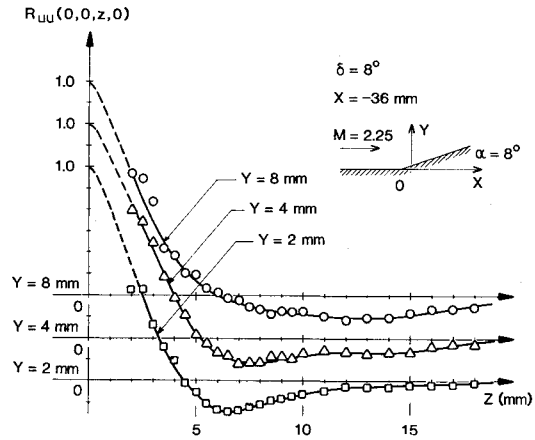

Fig. 17 Evolution of the lateral correlation function of the longitudinal mass flux fluctuations with distance from the wall in the undisturbed boundary layer.

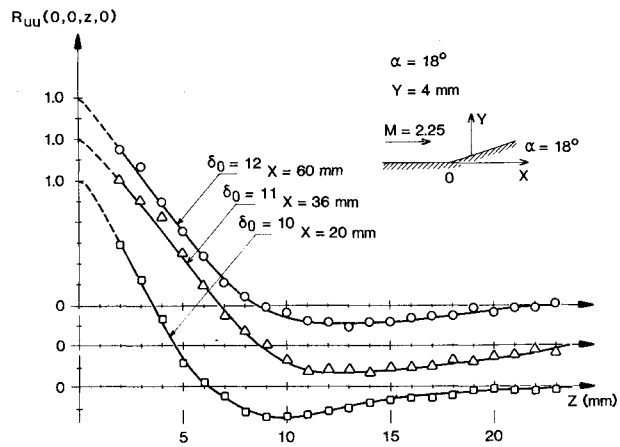

Fig. 18 Evolution of the lateral correlation function with the longitudinal distance in the interacting boundary layer (distance from the wall = 4 mm).

$y = 8$ mm. The maximum negative value can reach -0.15. The existence of a rather well-organized lateral pattern of turbulent structures is suggested, with contiguous contrarotating vortices. The increasing width of the curves with height is related to the diminution of the number of small-scale structures with distance from the wall.

The evolution of the correlation function with the distance x from the hinge of the compression corner of 18 deg angle is presented in Fig. 18. The height y is held fixed at 4 mm from the wall. The width of the curves increases with distance. The Δz corresponding to $C_{\rho u', \rho u'} = 0$ grows from 5 mm at the start of the interaction to 8 mm downstream of $x = 36$ mm. The negative part of the function remains clearly discernible.

III. Discussion of Results and Conclusion

The turbulent properties of the flowfield in a supersonic shock-wave/boundary-layer interaction have been investigated by means of the available experimental tools: pressure survey, laser Doppler and hot-wire anemometers, and schlieren visualization. Although some details of the experimental procedures are related in the paper and could be discussed here, the conclusions will be devoted to the results concerning the turbulent properties. From the hot-wire data and optical visualizations, two important conclusions may be drawn:

1) A large amount of the turbulent energy is contained in large-scale structures that are not destroyed along the length of the interaction process, but rather reactivated. A typical scale may be defined, which is 2δ in the flow direction and δ in the other directions. The existence of a lateral contrarotating pattern of turbulent eddies is strongly suggested.

2) A low-frequency component in the turbulent frequency spectrum is observed in the vicinity of the separation bubble. This feature may be associated with an unsteadiness of the separation bubble itself which does not affect the rest of the flow.

A phenomenological observation may be made from LDA data:

3) The shear component of the Reynolds stress tensor, $\overline{u'v'}$ increases more rapidly than the normal components $\langle u' \rangle^2$ and $\langle v' \rangle^2$ in the first part of the interaction and decreases more rapidly further downstream. The second feature may be easily explained since the turbulent motion involves large-scale eddies that cannot dissipate within the length investigated, but can loose their coherence. The first feature is less obvious and suggests a tendency toward an organization of the turbulent structures related to the deceleration of the inner part of the boundary layer.

From a more computational point of view, two properties may be noted:

4) The normal static pressure gradient inside the boundary layer is moderate, at least for regions not too close to the shock wave. A computation based on the boundary-layer equations seems valid at moderate Mach numbers when the compression waves coalesce in the outer part of the boundary layer.

5) In the vicinity of the separation bubble, the shear stresses are not large and the spatial derivatives of the normal stresses, especially $\partial \langle u' \rangle^2 / \partial x$ contribute significantly to the momentum balance. At $y = 1$ mm, $\langle u' \rangle^2 / u_\infty^2$ decreases by nearly 50% between $x = -4$ and $+4$ mm. This observation is in agreement with the result obtained by Simpson[18] in a subsonic separating boundary layer.

As a general conclusion, it may be said that the modeling of the turbulence in the shock wave/boundary layer probably requires a deeper insight into the mechanisms of turbulence than our current knowledge provides. The reason is that the overall longitudinal scale length of the phenomenon is very close to the scale of the turbulent eddies, which suggests a strong nonlinear coupling between the mean flow and the turbulent structures.

References

[1]Shang, J. S. and Hankey, W. L., "Numerical Solution of the Navier-Stokes Equations for Supersonic Turbulent Flow over a Compression Ramp," AIAA Paper 75-3, 1975.

[2]Hung, C. M. and MacCormack, R. W., "Numerical Solution of Supersonic and Hypersonic Turbulent Compression Corners Flows," *AIAA Journal*, Vol. 15, March 1976, pp. 410-416.

[3]Rubesin, M. W., Crisalli, A. J., Horstman, C. C., and Acharya, M., "A Critique of Some Recent Second Order Closure Models for Compressible Boundary Layers," AIAA Paper 77-128, 1977.

[4]Chapman, D. R., Kuehn, D. M., and Larson, M. K., "Investigation of Separated Flows in Supersonic and Subsonic Stream with Emphasis on the Effect of Transition," NACA TN 3869, 1957.

[5]Kussoy, M. I., Horstman, C. C., and Acharya, M., "An Experimental Documentation of Pressure Gradients and Reynolds Number Effects on Compressible Turbulent Boundary Layers," NASA TM 78-488, 1978.

[6]Mikulla, V. and Horstman, C. C., "Turbulence Measurements in Hypersonic Shock Wave Boudnary Layer Interaction Flows," *AIAA Journal*, Vol. 14, May 1976, pp. 568-575.

[7]Rose, W. C. and Johnson, D. A., "Turbulence in Shock Wave Boundary Layer Interaction," *AIAA Journal*, Vol. 13, July 1975, pp. 884-889.

[8]Delery, J., Copy, C., and Reisz, J., "Analyse en velocimétrie Laser bidirectionnel d'une interaction choc-couche limite turbulente avec decollement étendu," ONERA Rept. 37/7078 AY 014, 1980.

[9]Mateer, G. G., Brosh, A., and Viegas, J. R., "A Normal Shock-Wave Turbulent Boundary Layer Interaction at Transonic Speeds," AIAA Paper 76-161, 1976.

[10]Ardonceau, P., "Etude de l'interaction onde de choc-couche limite supersonique," Thèse 343, Université de Poitiers, France, 1981.

[11]Settles, G. S., Fitzpatrick, T. J., and Bogdonoff, S. M., "Detailed Study of Attached and Separated Compression Corner Flowfields in High Reynolds Number Supersonic Flow," *AIAA Journal*, Vol. 17, June 1975, pp. 573-585.

[12]Ardonceau, P., Lee, D. H., Alziary, Th., and Goethals, R., "Turbulence Behaviour in a Shock Wave-Boundary Layer Interaction," AGARD CP 271, 1978.

[13]Korkegi, R. H., "Comparison of Shock Induced Two- and Three-Dimensional Incipient Turbulent Separation," *AIAA Journal*, Vol. 13, April 1974, pp. 534-535.

[14]Lennert, A. E., Brayton, D. B., Crosswy, F. L., Goethert, W. H., and Kalb, H. T., "Laser Metrology," AGARD LS 49, 1971.

[15]Yanta, W. J., "Use of the LDV in Subsonic and Supersonic Flow," Project Squid, Purdue University, West Lafayette, Ind., 1972.

[16]Johnson, D. A. and Rose, W. C., "Laser Velocimeter and Hot Wire Anemometer Comparison in a Supersonic Boundary Layer," *AIAA Journal*, Vol. 13, April 1975, pp. 512-515.

[17]Quigley, M. S. and Tiederman, W. G., "Experimental Evaluation of Sampling Bias in Individual Realization Laser Anemometry," *AIAA Journal*, Vol. 15, Feb. 1977, pp. 266-268.

[18]Simpson, R. L., et al., "The Structure of a Separating Turbulent Boundary Layer," *Journal of Fluid Mechanics*, Vol. 113, Dec. 1981, pp. 23-90.

[19]Morkovin, M. V., "Fluctuations and Hot Wire Anemometry in Compressible Flow," AGARDograph No. 24, 1956.

[20]Kovasznay, L.S.G., "Turbulence in Supersonic Flow," *Journal of the Aeronautical Sciences*, Vol. 20, Oct. 1953, pp. 657-682.

[21]Lee, D. H., "Etude de l'évolution de la turbulence dans une interaction onde de coc-couche limite," These, Université de Poitiers, France, 1979.

[22]Demetriades, A. "Turbulence Measurements in an Axisymmetric Compressible Wake," Philco-Ford Corp., Rept. TR No. UG-4118, 1967.

[23]Bonnet, J. P. and Alziary, Th., "Determination and Optimization of Frequency Response of Constant Temperature Hot Wire Anemometers in Supersonic Flows," *Review of Scientific Instruments*, Vol. 51, Feb. 1980, pp. 234-239.

[24]Rose, W. C. and McDaid, E. P., "Turbulence Measurements in Transonic Flow," *AIAA Journal*, Vol. 15, Sept. 1977, pp. 1368-1370.

[25]Hinze, J. O., *Turbulence*, McGraw Hill Book Co., New York, 1959.

[26]Grande, E. and Oates, G. L., "Unsteady Flow Generated by Shock-Turbulent Boundary Layer Interactions," AIAA Paper 73-168, 1973.